JOURNAL OF MATERIALS SCIENCE 26 (1991) 4208–4214

Application of an indentation method to the fracture mechanics study of a polycrystalline graphite

T. MIYAJIMA, M. INAGAKI, M. SAKAI
Department of Materials Science, Toyohashi University of Technology, Tempaku-cho, Toyohashi 441, Japan

None of the conventional indentation techniques are applicable to carbon and graphite materials for determining fracture mechanics parameters because of the difficulty in introducing well-defined median/radial cracks. A novel indentation method is proposed in this work for fracture mechanics studies and then applied to a polycrystalline graphite fracture. The most prominent advantage of the indenter designed is that the residual stresses beneath the indentation impression, which prevail in conventional indentation methods (Knoop and Vickers indentations) and lead to crucial difficulties in fracture mechanics analysis, are negligibly small. This makes possible a quantitative study on the microstructural interaction between the indentation-induced micro-flaw and the natural intrinsic flaws of the material. The dependence of flexural strength of a polycrystalline graphite on the indentation-induced surface flaw size is also discussed by examining the microstructural scaling transition of fracture origin from the indentation-induced to the intrinsic flaws with diminishing indentation surface flaw. An important role of the Mrozowsky micro-crack system in the scaling transition is emphasized.

1. Introduction

Numerous fracture mechanics techniques are available for studying the fracture behaviour of polycrystalline graphite materials, among which both compact tension (CT) and single edge-notched bend (SENB) methods are most conventional in laboratory work, not only because of the ease of machining and testing but also because exact expressions exist for their stress intensity factors (K_I) as a function of crack length [1]. Both CT and SENB specimens are classified as "macro-notched" from the viewpoint of the dimension of the notch introduced, in contrast to "micro-cracked" specimens with micro-flaws induced by indentation methods. One of the most significant advantages of micro-flaw techniques is that the toughness can be measured for flaws with a similar size to the strength-controlling natural flaws existing in the microstructure of the material. A prominent difference must be recognized between fracture processes taking place at macro-crack and micro-flaw fronts. The micro-crack front passes only a few grains at incipient cracking, while the macro-crack front encounters numerous grains and grain boundaries not only at incipient cracking but also during crack extension. Hence, the information obtained from indentation-induced micro-flaws will be more straightforward and significant in some cases for discussing the fracture behaviour of strength-controlling natural flaws in brittle materials than that obtained from macro-notched specimens. In fact, a finite difference in fracture toughness values obtained from macro- and micro-cracks has been reported in some ceramic systems [2] because of a significant difference in microstructural interactions at macro- and micro-crack tips [3, 4].

Surface flaws with controlled size and shape can be introduced into a brittle material by a sharp hardness indentation [5–7]. Two major indenter geometries for introducing controlled surface flaws have been the Knoop and Vickers configurations, for they are commercially available. The Knoop indentation gives the damage of a single crack, which makes it more amenable to fracture mechanics application to a surface flaw [8]. The Vickers geometry, which produces two cracks at right-angles, makes it much easier to introduce well-defined surface flaws on a brittle material surface, though the stress–strain field around the indentation impression is rather more complicated than that of Knoop. The dimensions of the impression and the flaws induced are readily controlled to a high degree of reproducibility by controlling the contact load.

A specific feature of the sharp indenter pattern is the plastic central zone and associated residual stresses beneath the immediate contact area [9]. A major concern in indentation-induced micro-crack techniques for determining fracture toughness has been how to deal with the residual stress field produced by the indentation, because of the very complex elastic/plastic stresses generated in these crack systems [10, 11].

0022–2461/91 $03.00 + .12

Micro-flaw techniques for determining fracture toughness are basically classified into two categories: one is the controlled surface flaw (CSF) method [12], and the other includes the indentation microfracture (IM) [13–15] and indentation strength-in-bending (ISB) [16] techniques. The former technique (CSF) has a well-defined expression for the stress intensity factor (K_I) of the micro-flaw [12] which makes the fracture toughness determination quantitative, if the residual stress induced by the indentation can be removed completely in advance of the fracture toughness test [12]. It is always applicable when the shape and dimensions of the indentation-induced surface flaws are defined well in the fracture test. The latter techniques (IM and ISB), on the other hand, are always based on semi-empirical expressions [13–16] which lead to a qualitative evaluation of the fracture toughness in some brittle ceramics, and to difficulty in their application to some other ceramic materials including carbon, graphite and their composite materials.

The most attractive advantage of the IM method may be in the specimen size requirement, dimensions as small as 5 mm × 5 mm × 5 mm being enough for determining the fracture toughness. In addition, the IM method does not require any time-consuming and complicated procedures for machining the fracture mechanics test specimens. An optically smooth surface obtained by polishing is the only requirement before the fracture toughness test. However, it is almost impossible to use either the IM method or the ISB technique if the induced flaws cannot be identified as a well-defined median/radial or Palmqvist crack system. This suggests that the fracture toughness determined by IM or ISB methods should only be accepted with some degree of caution in the absence of any experimental identification of median/radial or Palmqvist crack systems. Upon applying indentation techniques to carbon and graphite materials for determining their fracture parameters, we are faced with a very crucial difficulty. The stress singularity at the sharp indenter tip of a Vickers or Knoop hardness tester introduces by no means well-defined median/radial or Palmqvist cracks into carbon and graphite materials. Even in glassy carbon, the most brittle carbon material, it is very difficult to generate indentation-induced radial cracks [17]. None of the conventional IM or ISB test designs can be applied to the toughness determination of any carbon or graphite material.

The major intent of the present work is to propose a modified indentation method for determining the fracture toughness, K_{Ic}, of a polycrystalline graphite material, and to address the microstructural interaction between strength-controlling micro-flaws and the graphite microstructure. In the novel indentation method used, troublesome procedures for notching and precracking are not required.

2. Experimental procedure

An isotropic polycrystalline graphite, IG-11 (Toyo Tanso Co. Ltd) was used for the present study. It was made of coke grains less than 15 μm in diameter and pitch binder through isostatic pressing, baking and then graphitization. The microstructural characteristics include a mean pore size of 5 μm, bulk density of 1.76 g cm^{-3} and a porosity of 15%.

Three-point bend specimens of width (W) = 8 mm, thickness (B) = 8 mm and length (L) = 72 mm were used for fracture mechanics tests. The tensile surface of the three-point bend specimen was polished to a mirror surface using emery papers (SiC, No. 600). In order to introduce a single controlled surface flaw on the polished surface, the novel sharp indenter shown in Fig. 1 was designed. The indenter tip was made of a hard steel plate (thickness = 0.5 mm) by machining a semi-circle (radius = 2.85 mm) with a sharp periphery (tip radius < 5 μm). This indenter is so thin and so sharp that the induced residual plastic stresses around the indentation flaw on the graphite surface are presumed to be negligibly small, which allows us to calculate the fracture toughness (K_{Ic}) without any of the ambiguities associated with compressive residual stresses induced by conventional indenters such as Knoop and Vickers. The surface flaw was generated by a hardness tester (Akashi Co. Ltd, AVK-AII). The relationship between the major and minor axes (c and a) of the semi-elliptical surface flaw introduced into the graphite surface is shown in Fig. 2. By changing the indentation load (P_i) from 200 g to 10 kg, the induced indentation flaw depth (a) was controlled from 20 to 640 μm. The indented surface flaw planes orient perpendicular to the tensile stress of the three-point bend configuration.

The flaw length ($2c$) was optically measured on the surface after indentation. Because of the difficulty in determining the precise flaw depth (a) on the fracture surface after the flexural test, a was calculated using the observed c-value and the following expression for a (mm) and c (mm) of the indenter ellipse (see Fig. 2):

$$a = 2.85 - (2.85^2 - c^2)^{1/2} \quad (1)$$

Three-point flexural tests were conducted over a loading span (S) of 60.0 mm (S/W = 7.5) at room temperature in air. The displacement-controlled testing

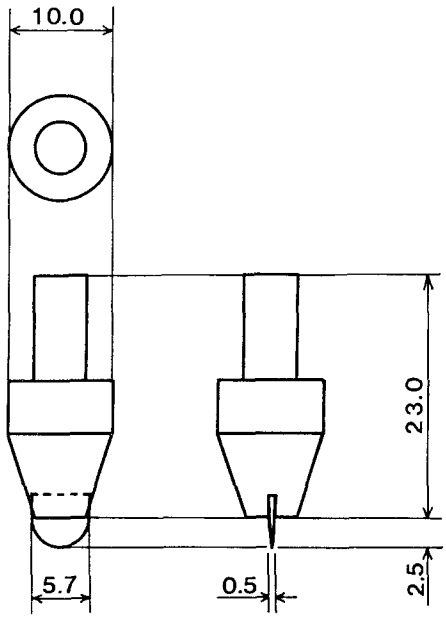

Figure 1 Semi-circular indenter design (dimensions in mm).

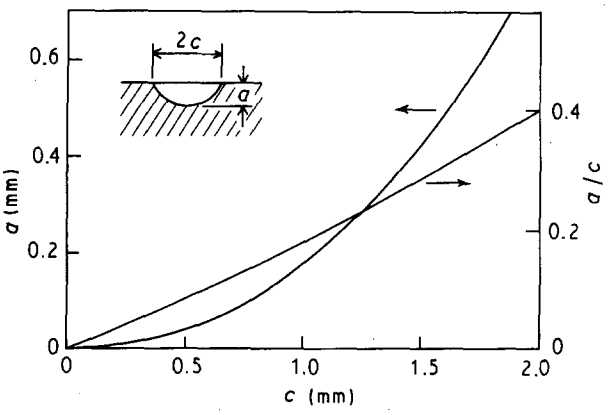

Figure 2 Interrelationship between major and minor axes (c and a) of the surface flaw generated by the indenter.

machine was operated at a crosshead speed of 0.5 mm min^{-1}.

The flexural strength (σ_f) was calculated from

$$\sigma_f = 3P_f S/2BW^2 \quad (2)$$

where P_f is the flexural load at failure and S, B and W are the loading span, thickness and width of the flexural specimen, respectively. The fracture toughness (K_{Ic}) was determined by the use of the strength (σ_f) of flexural specimens with a semi-elliptical indentation surface flaw via the following expression proposed by Newman and Raju [18]:

$$K_{Ic} = F(a/c, a/W)\,\sigma_f(\pi a)^{1/2} \quad (3)$$

where the shape factor, $F(a/c, a/W)$, is 0.90 ± 0.03 for $0.1 < a/c < 0.35$ and $a/W \ll 1$. The numerical detail of the shape factor is given in the stress intensity factors handbook [19]. It was confirmed by comparing the obtained fracture toughness values with those evaluated with conventional fracture mechanics specimens (SENB and CT specimens) that the residual compressive stresses around the indented surface flaw have no effect on the toughness value measured.

3. Results

The interrelationship of indentation load (P_i) with the induced surface flaw size (half-length of major axis (c) of the semi-ellipse) is demonstrated in Fig. 3. The log$c$ versus logP_i relation is described by a straight line with a slope of 0.42. This is completely different from the values for median/radial and Palmqvist crack systems induced in brittle ceramics by a Vickers indentation, where the slope should (for example) be 2/3 for the median/radial crack system.

The flexural strength (σ_f) versus flaw size (a) relation is plotted in Fig. 4. Open and solid circles stand for failures from the indentation flaws and from inherent natural defects (flaws), respectively. The hatched zone on the ordinate marks the variation of the strength (σ_f^*) controlled by inherent natural flaws. The broken line having a slope of $-\frac{1}{2}$ is calculated from Equation 3 assuming a fracture toughness (K_{Ic}) of 0.90 MPa m$^{1/2}$. A well-known fracture mechanics rule, i.e. $\sigma_f \propto 1/a^{1/2}$, holds only in the range of sufficiently large flaw size ($a > 0.5$ mm). The log σ_f versus log$a$

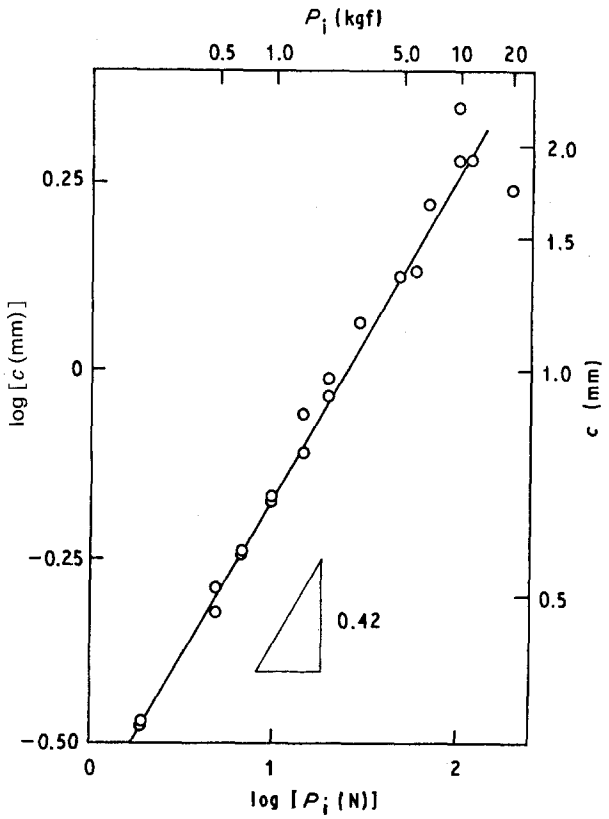

Figure 3 Dependence of the induced flaw size (c) on the indentation load (P_i).

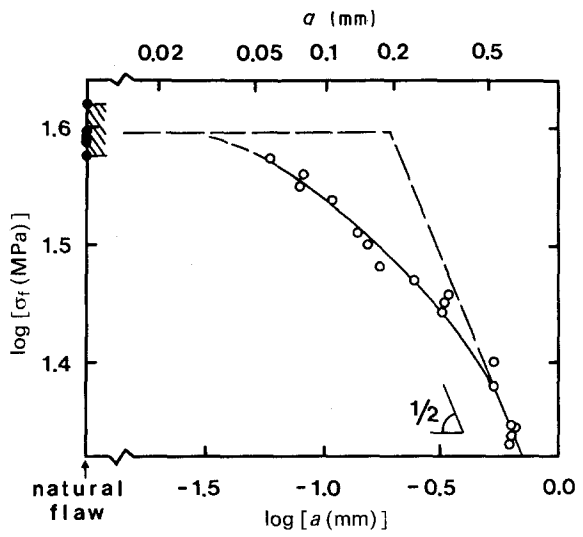

Figure 4 Flexural strength change (σ_f) with the depth (a) of indentation-induced surface flaw. Closed circles and the hatched region on the ordinate are, respectively, the flexural strength and its variation for failures from intrinsic natural flaws.

relation deviates from the $\frac{1}{2}$ power law with decreasing flaw size. It is likely to converge to a strength plateau in the limit of a small flaw. This plateau strength coincides with the inherent strength, σ_f^*.

4. Discussion

4.1. Fracture toughness, K_{Ic}

Two of the present authors and their co-workers [20–22] have studied extensively the determination of

fracture mechanics parameters (for example the fracture toughness (K_{Ic}), crack growth resistance (K_R), critical J-integral (J_{Ic}) and the potential energy-derived fracture toughness (R)) for polycrystalline graphite materials using conventional fracture mechanics specimens with a "macro-notch", such as CT and SENB specimens. The major results obtained so far for the present polycrystalline graphite (IG-11) are:

(a) the fracture toughness, K_{Ic}, determined at "crack initiation" is 0.74 ± 0.11 MPa $m^{1/2}$;

(b) the Irwin similarity relation $J_{Ic} = K_{Ic}^2/E'$ holds, while the load–displacement relation is not linear even for loads much less than the failure load;

(c) the historical dependence of crack-growth resistance (K_R), which has been referred to as "R-curve" behaviour, exists. There is a rapidly rising R-curve behaviour at the initial stage of crack extension ($0 < \Delta a < 1.5$ mm), followed by a toughness plateau (K_c^∞) at about 1.2 MPa $m^{1/2}$; and

(d) the rising behaviour is dominated by grain bridging tractions between fracture surfaces developed behind a propagating crack tip. The toughness plateau corresponds to a steady-state crack bridging.

The above results (c) and (d) on the rising behaviour of crack growth resistance (K_R) implies that the apparent fracture toughness, $K_Q(P_{max})$, which is conventionally determined by the use of peak load (P_{max}) or a load for unstable failure, is always somewhat larger than the "true" fracture toughness, K_{Ic}, because of the finite extent of stable crack growth (Δa) before reaching P_{max}. The K_Q value must fall between K_{Ic} ($= 0.74$ MPa $m^{1/2}$) and K_c^∞ ($= 1.2$ MPa $m^{1/2}$). In fact, the K_Q values measured on SENB and CT specimens at failure load are 0.9 ± 0.1 and 1.1 ± 0.1 MPa $m^{1/2}$, respectively, the difference being dependent on the difference in the crack growth stability for each specimen geometry which results in a difference in crack extension (Δa) before the load reaches P_{max}.

On applying the CSF method to fracture toughness measurement, we have to recognize the complication associated with rising R-curve behaviour, for the fracture toughness calculation must be conducted from the load for unstable failure (P_{max}) rather than for incipient crack extension (P_c), in addition to the compressive residual stress problem introduced by indentation. As shown, and described in the preceding section, the fracture toughness determined in the $\frac{1}{2}$-power law region in Fig. 4 is 0.90 ± 0.03 MPa $m^{1/2}$, in excellent agreement with values for the SENB design. We should note here that none of the treatments for eliminating residual stresses around the indentation-induced crack have been conducted in advance of fracture tests. This exhibits a significant contrast to the results of CSF techniques applied to ceramic materials with Vickers or Knoop indentation-induced surface flaws, where the residual stress around the indentation impression results in apparent toughness values of less than 30 to 40% of the true toughness [7, 12]. A good agreement between fracture toughness values obtained by the CSF method in the present work and by the conventional SENB method suggests that the residual stress induced by the present novel indenter tip (Fig. 1) is too insignificant to affect the experimentally determined fracture toughness. We should notice an important difference in the tip geometry between the present novel indenter and the Vickers or Knoop indenter: the former applies the indentation load on a sharp line, while the latter does so on a finite area which easily produces compressive residual stresses beneath the impression.

4.2. Microstructural interaction between indentation-induced and intrinsic microflaws

As represented by the Mrozowsky crack system, polycrystalline graphite materials have numbers of microcracks, defects and micropores with a wide range of dimensions and geometries [23, 24]. These microcracks comprise intrinsic cracks and pores included in filler coke grains as well as those formed by thermal mismatch and crystallographic volume change, induced by both carbonization and graphitization processes. The dimensions of microcracks range from 0.01 to 500 μm in high-density polycrystalline graphites with a fine microstructure. The strength-controlling microcracks must be the largest (weakest) cracks of all cracks pre-existing in the microstructure. The dimensions of the weakest crack, i.e. the strength-controlling natural crack of the present graphite (IG-11), can be estimated from the flexural strength ($\sigma_f^* = 38$ MPa) of a non-indented specimen with a smooth surface and the fracture toughness ($K_{Ic} = 0.90$ MPa $m^{1/2}$) through the fracture mechanics equation (Equation 3), yielding $a^* = 0.2$ mm and $c^* = 1.0$ mm as an equivalent surface flaw (the semi-elliptical surface crack illustrated in Fig. 2). It is very interesting to note that the strength-controlling natural flaw sizes (a^* and c^*) have the same order of magnitude as those of indentation-induced surface flaws in the CSF method used in this work, i.e. $0.02 < a < 0.7$ mm and $0.34 < c < 1.8$ mm.

As stressed in the foregoing section, with progressively diminishing indentation-induced flaw size, a deviation from the $\frac{1}{2}$-power law in the $\log \sigma_f$ versus $\log a$ relation (see Fig. 4) is observed, followed by a strength plateau. In this regime of microstructural scaling transition, the failure strength (σ_f) is generally described by

$$\sigma_f = \frac{\eta(a) K_{Ic}(\text{macro})}{F(\pi a)^{1/2}} \tag{4}$$

where the frontal factor, $\eta(a)$, describes the details of scaling transition behaviour, that is the "path of transition". The shape factor of the flaw is given by F. K_{Ic}(macro) stands for the fracture toughness determined by the use of a crack or flaw large enough compared to the size of natural flaws which control the intrinsic strength, i.e. $a \gg a^*$. An alternative expression for the scaling transition in the σ_f versus a relation in the region $a \approx a^*$ may be made by using the apparent flaw size, a_{app}:

$$\sigma_f = \frac{K_{Ic}(\text{macro})}{F(\pi a_{app})^{1/2}} \tag{5}$$

where a_{app} is linked to the real crack size (a) by $a_{app} = a/\eta^2(a)$.

In the diminishing flaw region ($a \ll a^*$), the natural flaw (a^*) dominates the failure strength, thence giving the strength plateau at σ_f^*:

$$\sigma_f^* = \frac{K_{Ic}(\text{micro})}{F(\pi a^*)^{1/2}} \tag{6}$$

where K_{Ic} (micro) is the fracture toughness which controls the critical load or stress level for unstable crack extension of the inherent micro-flaw. The difference between K_{Ic} (macro) and K_{Ic} (micro) comes basically from the differences in fracture processes and mechanisms which occur at macrocrack and microcrack fronts of polycrystalline materials, as discussed in the preceding section.

Consider an indentation-induced surface flaw with a depth a on a polished surface of polycrystalline graphite. If the indentation flaw size (a) is sufficiently larger than that of the inherent natural flaw, a^*, then the failure strength (σ_f) is evidently controlled by the indentation flaw; the macroscopic fracture toughness, K_{Ic} (macro), which reflects the normal polycrystalline fracture process, will be supposed to determine the critical stress for unstable crack extension as described by

$$\sigma_f = \frac{K_{Ic}(\text{macro})}{F(\pi a)^{1/2}} \tag{4'}$$

In the extreme of $a \ll a^*$, on the other hand, it is assumed that the inherent flaw (a^*) dominates the graphite strength, so that the failure may be described by the microscopic fracture toughness (K_{Ic} (micro)) reflecting the critical crack surrounded by few grains, the failure strength being described by Equation 6.

This phenomenological consideration of two extreme cases of the strength versus flaw-length relation leads again to the important notion of a scaling transition of the fracture origin at $a \approx a^*$ from a to a^*. A possible expression which unifies the σ_f versus a relation over a wide range of flaw size might be developed by combining the two extreme strength–flaw-size relationships: Equation 4′ for $a/a^* \gg 1$ and Equation 6 for $a/a^* \ll 1$, and considering the "path of transition":

$$\sigma_f = \frac{K_{Ic}\,(\text{macro})}{F[\pi(a + \tilde{a}^*)]^{1/2}} \tag{7}$$

where the characteristic flaw size, $\tilde{a}^*$, is given by

$$\tilde{a}^* = k^2 I(a/a^*)a^* \tag{8}$$

using the true value (a^*) of the strength-controlling inherent flaw size. In Equation 8, $k \equiv K_{Ic}$ (macro)/K_{Ic} (micro), and the microstructural interaction function, $I(a/a^*)$, is a dimensionless function varying from 0 (for $a/a^* \gg 1$) to 1 (for $a/a^* \ll 1$). Equation 7 satisfies both the extreme expressions of Equations 4′ and 6 as well as the "path of transition" through the interaction function, $I(a/a^*)$.

We have no physical insights into the functional form of $I(a/a^*)$ for the present graphite material. However, the empirical determination of the $I(a/a^*)$ function and an insight into its physical significance aid an understanding of the essential role of the polycrystalline graphite microstructure (Mrozowsky crack system) in the relationship of strength with flaw size. The experimentally fitted solid curve in Fig. 4 combined with Equations 7 and 8 provide the empirical $I(a/a^*)$ function for the graphite as demonstrated in Fig. 5, where use has been made of the assumption that K_{Ic} (micro) = K_{Ic} (macro) (= 0.90 MPa m$^{1/2}$) for simplicity.

Comparing Equation 7 with Equation 5, the apparent flaw depth (a_{app}) can be expressed by

$$a_{app} = a + \tilde{a}^* \tag{9}$$

It is always larger than the true crack length, a, i.e. $a_{app} > a$ whenever microstructural interaction exists because $\tilde{a}^* \geqslant 0$ via $k \geqslant 0$ and $I(a/a^*) > 0$ in Equation 8; microstructural interaction then results in a strength somewhat lower than that estimated from the true crack length, a, namely, the deviation from the $\frac{1}{2}$-power law in Fig. 4 with decreasing flaw dimension arises.

The increased apparent crack length a_{app} may reflect the coalescence of cracks a and a^* through a microfracture mechanics interaction. The extent of this interaction is evidently affected by the geometrical separation, $r(a, a^*)$, between these cracks, a and a^*, two of the extreme cases being shown in Fig. 6a for a dilute intrinsic crack system where $r(a, a^*) \gg a$ and a^*, and Fig. 6b for a concentrated crack system where $r(a, a^*) \approx a$ and a^*. In the former crack system, the flaw (a) introduced at the surface seldom meets geometrically with the intrinsic natural flaws (a^*), implying no fracture mechanics interactions with each other; there is then a sharp transition in the strength at $a = a^*$ from the $\frac{1}{2}$-power law region ($\sigma_f \propto /a^{1/2}$) to the strength plateau at $\sigma_f = \sigma_f^*$ (see broken lines in Fig. 4), corresponding to the sharp transition of the strength-controlling flaw from a to a^* [25]. In such a non-interacting crack system, the $I(a/a^*)$ function should be expressed by using the Heaviside step function $H(x)$:

$$I\left(\frac{a}{a^*}\right) = \left(1 - \frac{a}{a^*}\right)H\left(1 - \frac{a}{a^*}\right) \tag{10}$$

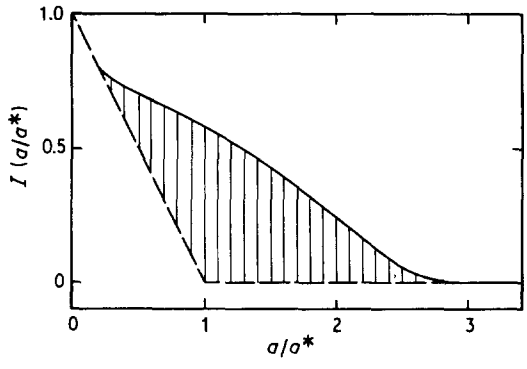

Figure 5 Interaction function $I(a/a^*)$ (Equation 8) for polycrystalline graphite. Broken lines represent the $I(a/a^*)$ function of the non-interacting system. The hatched area demonstrates the microstructural interaction between strength-controlling flaws in the graphite.

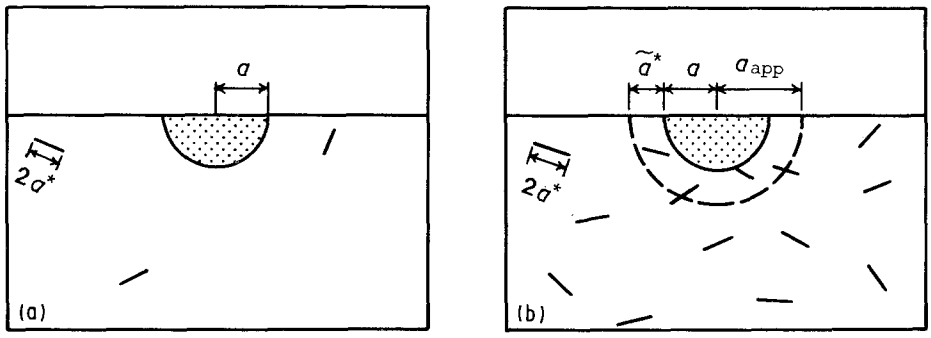

Figure 6 Apparent flaw concept and microstructural interaction between the indentation-induced surface flaw and the intrinsic flaws in (a) a dilute (non-interacting) and (b) a concentrated (interacting) crack system.

where $H[1 - (a/a^*)]$ becomes zero for $a/a^* > 1$ and unity for $a/a^* < 1$, and use has been made of the assumption that $k = 1$. The $I(a/a^*)$ function of Equation 10 is shown in Fig. 5 by broken lines. The difference between the observed (solid line) and the non-interacting transitions (broken lines) which is marked by a hatched area demonstrates the microstructural interaction existing in our polycrystalline graphite material.

The apparent flaw in a concentrated crack system depicted in Fig. 6b typifies the microstructural interaction between the indentation induced crack and the intrinsic Mrozowsky crack system of our graphite. The increment in the apparent flaw size, Δa ($= a_{app} - a \equiv \tilde{a}^*$), not only includes the real dimension of the intrinsic flaw (a^*) but also reflects the microfracture mechanics effect.

Cook *et al.* [26] have made a study of the strength characteristic as a function of the relation of crack size to grain size, using controlled Vickers indentation flaws in polycrystalline aluminas, barium titanates and glass ceramics. With progressively diminishing indentation load, they observed a steady increase in strength followed by a strength plateau as the crack size approached the characteristic grain size, similar to the strength transition in the present work. To describe this transition, they extended the conventional ISB technique to account for the microstructural effect by introducing a "micro-structural driving force", and then concluded the existence of a "microstructural R-curve", signifying a steady decrease in apparent fracture toughness with diminishing indentation-induced flaw size. A similar study addressing this microstructural R-curve behaviour was also conducted by Usami *et al.* [27]. In contrast to these apparent fracture toughness approaches to the microstructural scaling transition in the strength versus flaw-size relationship, apparent (or effective) crack length approaches as investigated in the present work have been conducted by Neuber [28], Smith [29] and Tanaka [30]. The most essential feature of our model is that the transition of the strength-controlling fracture origin is included explicitly in the apparent flaw-size approach.

5. Conclusion

As is well known in the application of the indentation method to fracture toughness determination, the indentation-associated plastic residual stresses around the impression always bring difficulties in the fracture mechanics analysis. In addition, upon applying the indentation technique to carbon and graphite materials, the sharp indenter tip of a Vickers or Knoop hardness tester makes by no means a well-defined medial/radial crack system, implying that none of the conventional IM and ISB test designs are applicable to toughness determination.

To overcome these difficulties in carbon and graphite fracture science and engineering, a sharp indenter tip with a thin semi-circular plate having a sharp periphery was designed. It applies the indentation load on a sharp line of the specimen surface, instead the conventional Knoop and Vickers load on a finite area. It was revealed that the line-like impression introduced to the surface of polycrystalline graphite material does not produce plastic residual stresses around the impression, making it possible to determine the fracture toughness by the CSF technique without polishing the residual stresses out of the indented surface. Because of the absence of indentation-induced residual stresses, microstructural interaction between the indentation and the natural flaws could be qualitatively studied by examining the dependence of the flexural strength (σ_f) of a polycrystalline graphite on the indentation-induced surface flaw size (a). The strength changes with $1/a^{1/2}$ in the region of large flaws ($a > 0.5$ mm), whilst it deviates from the $1/a^{1/2}$ relation with progressively diminishing indentation-induced flaw size, converging to a plateau in strength. The transition in strength from the $1/a^{1/2}$ regime to the plateau results from the transition in the strength-controlling flaw from the indentation-induced flaw (a) to the intrinsic natural flaw (a^*) of the graphite.

The micromechanics interaction between a and a^* dictates the "path of transition" in the strength versus flaw size relation. In this work, the apparent flaw concept was applied to discussing the micromechanics interaction of strength-controlling flaws.

Acknowledgement

This work was completed with support from the Japan Ministry of Education under a Grant-in-Aid for Scientific Research (No. 01 550 598).

References

1. ASTM Standard E399-83 in "Annual Book of ASTM Standards" (American Society for Testing and Materials, Philadelphia, 1983).
2. J. J. MECHOLSKY Jr, S. W. FREIMAN and R. W. RICE, *J. Mater. Sci.* **11** (1976) 1310.
3. R. W. RICE, S. W. FREIMAN and J. J. MECHOLSKY Jr, *J. Amer. Ceram. Soc.* **63** (1980) 129.
4. J. J. MECHOLSKY and S. W. FREIMAN, in "Fracture Mechanics Applied to Brittle Materials", edited by S. W. Freiman, ASTM STP 678 (American Society for Testing and Materials, Philadelphia, 1979) p. 136.
5. J. G. P. BINNER and R. STEVENS, *Trans. J. Br. Ceram. Soc.* **83** (1984) 168.
6. P. OSTJIC, *Int. J. Fract.* **33** (1987) 297.
7. B. R. LAWN, *Fract. Mech. Ceram.* **5** (1983) 1.
8. D. B. MARSHALL, *J. Amer. Ceram. Soc.* **66** (1983) 127.
9. A. G. EVANS and T. R. WILSHAW, *Acta Metall.* **24** (1976) 939.
10. B. R. LAWN and R. WILSHAW, *J. Mater. Sci.* **10** (1975) 1049.
11. B. R. LAWN, A. G. EVANS and D. B. MARSHALL, *J. Amer. Ceram. Soc.* **63** (1980) 574.
12. J. J. PETROVIC and M. G. MENDIRATTA, in "Fracture Mechanics Applied to Brittle Materials", edited by S. W. Freiman, ASTM STP 678 (American Society for Testing and Materials, 1979) p. 83.
13. B. R. LAWN, A. G. EVANS and D. B. MARSHALL, *J. Amer. Ceram. Soc.* **63** (1980) 574.
14. G. R. ANSTIS, P. CHANTIKUL, B. R. LAWN and D. B. MARSHALL, *ibid.* **64** (1981) 533.
15. K. TANAKA, *J. Mater. Sci.* **22** (1987) 1501.
16. P. CHANTIKUL, G. R. ANSTIS, B. R. LAWN and D. B. MARSHALL, *J. Amer. Ceram. Soc.* **64** (1981) 539.
17. H. HANYUU and M. SAKAI, unpublished work, 1989.
18. J. C. NEWMAN Jr and I. S. RAJU, NASA Technical Note TP-1578, Washington, D.C., 1979.
19. Y. MURAKAMI (ed.), "Stress Intensity Factors Handbook" (Pergamon, Oxford, 1987) p. 42.
20. M. SAKAI, K. URASHIMA and M. INAGAKI, *J. Amer. Ceram. Soc.* **66** (1983) 868.
21. M. SAKAI and R. C. BRADT, *Fract. Mech. Ceram.* **7** (1986) 127.
22. M. SAKAI, J. YOSHIMURA, Y. GOTO and M. INAGAKI, *J. Amer. Ceram. Soc.* **71** (1988) 609.
23. B. T. KELLY, "Physics of Graphite" (Applied Science, London, 1981) Ch. 6.
24. S. MROZOWSKY, in Proceedings of 1st and 2nd Carbon Conferences, Baltimore (Am. Carbon Soc, Buffalo, 1956) p. 31.
25. T. MIYAJIMA and M. SAKAI, *J. Europ. Ceram. Soc.* in press.
26. R. F. COOK, B. R. LAWN and C. J. FAIRBANKS, *J. Amer. Ceram. Soc.* **68** (1985) 604.
27. S. USAMI, H. KIMOTO, I. TAKAHASHI and S. SHIDA, *Eng. Fract. Mech.* **23** (1986) 745.
28. H. NEUBER, *Konstruction* **20** (1968) 245.
29. R. A. SMITH, *Int. J. Fract.* **13** (1977) 717.
30. K. TANAKA, *ibid.* **22** (1983) R39.

Received 30 March
and accepted 19 November 1990